

## **RADIOMETRIC CALIBRATION OF AIRBORNE LASER SCANNING DATA**

### **KALIBRACJA RADIOMETRYCZNA DANYCH Z LOTNICZEGO SKANINGU LASEROWEGO**

**Magdalena Pilarska**

Department of Photogrammetry, Remote Sensing and Spatial Information System,  
Faculty of Geodesy and Cartography, Warsaw University of Technology,

**KEY WORDS:** airborne laser scanning, LiDAR, multispectral laser scanning, radiometric calibration, OPALS

**ABSTRACT:** Airborne laser scanning (ALS) is widely used passive remote sensing technique. The radiometric calibration of ALS data is presented in this article. This process is a necessary element in data processing since it eliminates the influence of the external factors on the obtained values of radiometric features such as range and incidence angle. The datasets were captured with three different laser scanners; since each of these operates at a different wavelength (532, 1064 and 1550 nm) this makes the experiment more interesting. Radiometric calibration is a complex process, and a short theoretical background is therefore provided at the beginning of the article. The applied calibration procedure relies on areas with known reflectivity. The calibration regions should exhibit stable radiometric properties, therefore asphalt is used to calibrate each dataset and calculate a calibration constant for each flight block (wavelength) independently. Following this, the results of radiometric calibration, reflectance and backscattering coefficient, are presented and discussed in detail. Finally, the obtained reflectance values are compared with spectral characteristics. It could be shown that the reflectance values which result from radiometric calibration are similar to values presented on spectral characteristics.

#### **1. INTRODUCTION**

Airborne laser scanning (ALS) (Baltsavias, 1999) is a widely used technology in both photogrammetry and remote sensing. The main advantage of this method is primarily its fast and accurate data registration compared to other surveying methods. ALS data processing is also relatively fast when taking into account the area covered by the data. From ALS data various products can be generated, e.g., the digital terrain model (DTM), digital surface models (DSM) or even 3D city models (Wehr and Lohr, 1999). In recent years, multispectral laser scanning has become increasingly popular (Bakula, 2015). LiDAR technology consists in registering discrete data in more than one spectral band. There are laser scanners available on the market which operate within two or three bands simultaneously, e.g., Optech or Leica (Doneus *et al.*, 2015). In addition, bathymetric laser scanners are also available which operate only within a green band, e.g., Riegl systems

(Doneus *et al.*, 2015). This part of the spectrum allows for water penetration and is widely used in coastal zone mapping (Irish and Lillycrop, 1999).

If bathymetric laser scanner data is combined with near-infrared and shortwave-infrared lasers, the concept of multispectral laser scanning can be introduced. If data are registered in three different bands, more radiometric information are obtained, and this makes the ALS data more valuable and extends the possible applications. Multispectral laser scanning data, especially bathymetric systems, are applicable in archaeology. For shallow-water bodies, it is possible to map the underwater topography and to determine whether archaeological remains are present (Doneus *et al.*, 2015). In hydrography, bathymetric laser scanning is exploited in the monitoring of coastal changes, e.g., due to fluvial morphodynamics (Mandlbürger *et al.*, 2015) and water level changes. Another discipline in which multispectral laser data can be used is forestry, e.g., the green normalized difference vegetation index (green NDVI) calculation. This technique provides users with information on the distribution of the physiological processes of vegetation, and this allows a better understanding of the periodical changes in carbon content (Wallace *et al.*, 2012). According to Hemmler *et al.* (2006), terrestrial multispectral laser scanning can be used in detecting and classifying damages on building facades, e.g. moisture, biological covering. An experiment was conducted in which a wall was illuminated with a laser scanner registering on four different wavelengths (670, 808, 980 and 1930 nm). As a result, information about moisture, salinity and algae occurrence was obtained. Land cover classification, carried out by Wichmann *et al.* (2015), has also been based on multispectral data. Three datasets obtained in different spectral bands were integrated in such a way that every point had three intensity values, one its own and two assigned from neighbouring points. After supervised classification was carried out, the results of this study were acceptable. “Unsealed” ground point classification yielded an user accuracy of 95 % and “sealed” ground point: 74%.

The applications of multispectral laser scanning described above demonstrate the advantages and potential of this technology; many experiments and studies can make use of these relative intensity values. However, the intensity values are influenced by various factors such as range and incidence angle, and the obtained data therefore need to be calibrated in order to obtain radiometric measures for each echo which are independent from flight mission and sensor parameters (e.g. reflectance, backscattering coefficient). This article describes the radiometric calibration of three datasets obtained with different scanners, and the results are graphically presented and discussed. These values are then compared with spectral characteristics.

## 2. THEORETICAL BACKGROUND

The intensity registered by a laser scanner is influenced by many factors, for example range and incidence angle. Thus, radiometric calibration is necessary in order to eliminate or minimize the influence of these factors. The first part of the article provides a theoretical background regarding this radiometric calibration process.

In addition to geometric information, full-waveform LiDAR collects parameters such as amplitude and echo width. In order to fully exploit the potential of this data, radiometric calibration is required, to minimize the influence of these external factors. Two basic methods of radiometric calibration can be distinguished: relative and absolute intensity

correction (Briese *et al.*, 2012). Relative calibration consists of in minimizing the radiometric differences between strips, while absolute calibration consists in utilizing the radiometric measurements of the selected objects made using a reflectometer and calculating the calibration constant. These objects may be natural areas such as asphalt, or calibration targets characterized with a given brightness (Kaasalainen *et al.*, 2007).

The power of the pulse registered by the receiver of the laser sensor differs from the emitted power. This relation is described by the radar equation, which was adapted to ALS technology (Wagner, 2010):

$$P_r = \frac{P_t D_r^2}{4\pi R^4 \beta_t^2} \cdot \sigma \cdot \eta_{sys} \cdot \eta_{atm}, \quad \sigma = \frac{4\pi}{\Omega} \rho A_i \quad (1)$$

In Equation (1), the factors in the expression which affect the registered parameters are  $D_r$  (receiver aperture diameter),  $R$  (range, or distance between sensor and target),  $\beta_t$  (beam divergence),  $\eta_{sys}$  (system transmission factor),  $\eta_{atm}$  (atmospheric transmission factor),  $\sigma$  (backscatter cross section),  $\Omega$  (directionality of the scattering of the surface),  $\rho$  (reflectivity) and  $A_i$  (size of the area illuminated by the laser beam). The unknown parameters can be assumed to be constant and are replaced by a single variable, the calibration constant ( $C_{cal}$ ). In Equation (2), the received power  $\hat{P}_{tsp,i}$  is approximated by the product of the peak amplitude ( $\hat{P}_t$ ) times the echo width ( $s_{p,i}$ ) (Lehner and Briese, 2010):

$$\sigma = \frac{C_{cal} 4\pi R^4 \hat{P}_{tsp,i}}{\eta_{atm}}, \quad C_{cal} = \frac{\beta_t^2}{P_t D_r^2 \eta_{sys}} \quad (2)$$

The range, amplitude and echo width are the results of Gaussian decomposition from full-wave form registration. To calculate the calibration constant, the area of backscatter cross section is necessary. Assuming that illuminated area reflects the laser beam in accordance with Lambert's law, i.e., light is reflected equally in every direction, the area of the backscatter cross section can be calculated using Equation (1).

### 3. DATASETS

The datasets used in the experiment were obtained in an alluvial forest in Austria (Mandlbürger *et al.*, 2015a). The registered terrain forms part of the Natura2000 conservation area. The captured scene contains a gravel bed river, the surrounding alluvial forest as well as a national road and a railway line in the vicinity of the conservation area.

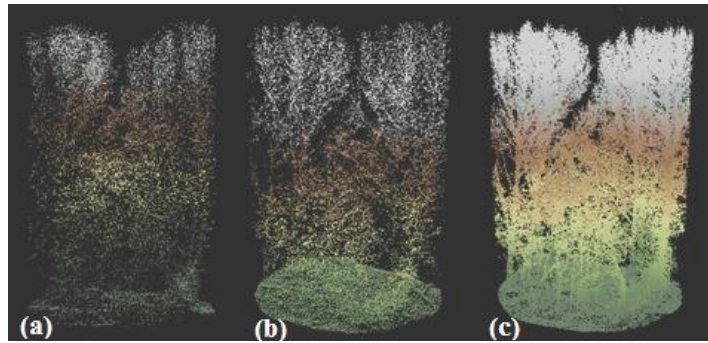


Fig. 1. Differences in point densities: (a)  $\lambda=532$  nm; (b)  $\lambda=1064$  nm (c)  $\lambda=1550$  nm

The three datasets obtained in this area (Mandlbürger *et al.*, 2015b) were radiometrically calibrated. The first was registered with a Riegl LMS-Q-1560 airborne laser scanner, which operates at a wavelength of 1064 nm, i.e., in the near-infrared spectrum. The second was collected with a bathymetric laser scanner, the Riegl VQ-880-G, although this was taken almost a month after the previous one. The third dataset was captured with an unmanned aerial vehicle (UAV) platform on which a Riegl VUX-1UAV was mounted. This laser scanner also operates in the near-infrared spectrum, but at a different wavelength ( $\lambda=1550$  nm); different properties are registered in this part of the spectrum compared with  $\lambda=1064$  nm. In addition to the differences in wavelength and operating altitude of the laser scanners, there was also a significant difference in the point densities (Fig. 1). The density of the bathymetric data was the lowest, while the density of the point cloud delivered by a UAV scanner can reach hundreds of points per square metre, and these differences mean that the experiment is more complex and interesting. The study area was approximately 0.12 km<sup>2</sup>.

#### 4. RADIOMETRIC CALIBRATION – RESULTS

Radiometric calibration is a complex process, which has already been described above with the theoretical background. This section presents the practical steps involved in the radiometric calibration of the given datasets and the results of this.

In practise, the first step in radiometric calibration is the selection of a calibration region, which should be characterized by stable radiometric properties. In most cases, man-made objects are the most appropriate choices. In this experiment, an asphalt surface was therefore chosen as a calibration region, and all points registered above the asphalt surface, e.g., cars or trees leaning towards the road, had to be removed. Furthermore, only those points which represented single echoes were used as the calibration region. The white traffic lines painted on the road also needed to be excluded, since these have different radiometric properties from asphalt. As a result, the calibration region was restricted to the traffic lanes (Fig. 2). The asphalt was chosen as the calibration region for all three datasets.

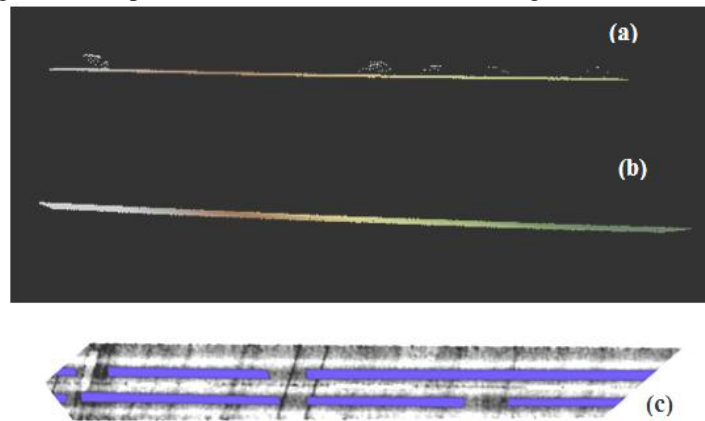


Fig. 2. Preparation of calibration region: (a) selected region; (b) calibration region after filtering; (c) restriction of the region to traffic lanes

The calibration constant was calculated using OPALS software (Pfeifer *et al.*, 2014), based on the given reflectance of the calibration region in each wavelength and the registered intensity of each echo. The reflectivity of the calibration region was assumed using the results of terrain measurements performed with a reflectometer. Based on the calculated calibration constant, the entire dataset could be calibrated, and the reflectance value and backscatter coefficient of every echo were obtained as a result.

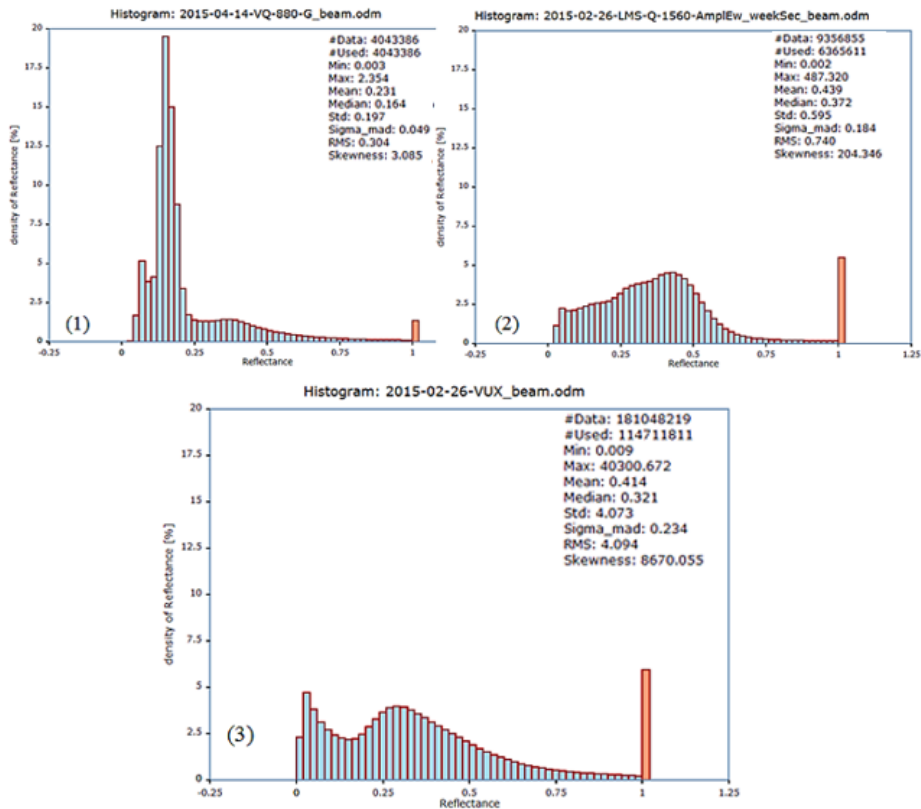


Fig. 3. Calibrated reflectance values of each dataset: (1)  $\lambda=532$  nm; (2)  $\lambda=1064$  nm  
(3)  $\lambda=1550$  nm

According to the histograms representing the calculated reflectance values, the reflectivity in the green spectrum is the lowest. Objects that reflect up to 25% of the radiation are in the majority. The reflection of most objects, and particularly vegetation, is much higher in the infrared spectrum than at the wavelength of green light. As a result, the mean value of reflectance for  $\lambda=1064$  nm was equal to 0.44, while at the green wavelength the reflectance was 0.23. These results are in line with the findings in Briese *et al.* (2012). For the dataset obtained by the UAV scanner, for which the wavelength was 1550 nm, the reflectance values presented in the histogram are similar to those for  $\lambda=1064$  nm. However, the reflection from vegetation in the third dataset is higher than in the green spectrum and somewhat lower than for dataset (2). An analysis of the histograms also shows that the variability in reflectivity for the infrared datasets is greater. A comparison of the reflectance

histograms also shows that the percentage of echoes for which the reflectivity is higher than one is different in each dataset. The percentage of these echoes is much higher in the infrared datasets (about 6%) than in the green one (2%). Presumably it can be caused by the Lambert's reflectance assumption. In practise, objects do not reflect the radiation ideally according to Lambert's law. Therefore, echoes with reflectance higher than one occurred. The results of the radiometric calibration were also presented as raster files, and these highlight the differences between the reflectivity properties of individual objects (Fig. 4).

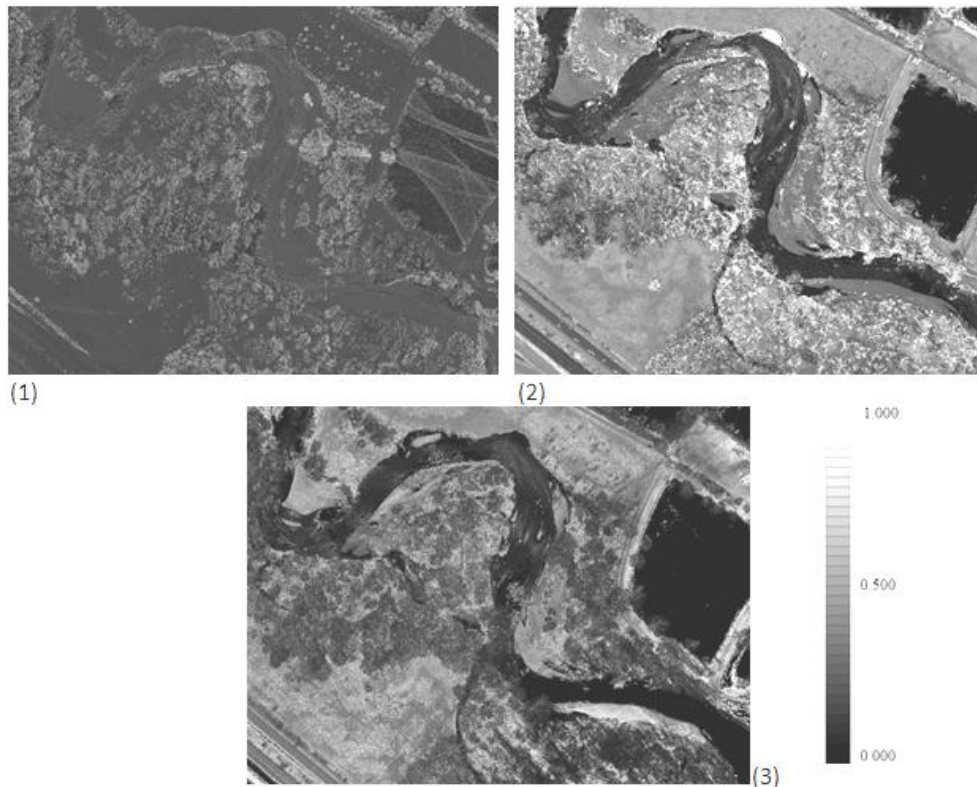


Fig. 4. Raster images representing reflectance values in each wavelength: (1)  $\lambda=532$  nm; (2)  $\lambda=1064$  nm; (3)  $\lambda=1550$  nm

Analysis of the reflectance rasters in Figure 4 gives rise to conclusions similar to those from the histograms. The reflectance is the lowest in the green spectrum, and highest for  $\lambda=1064$  nm; this confirms the value distributions in the histograms. Since the study area is mostly wooded, the differences in reflectance at the operating wavelengths can be clearly observed from the raster files.

In addition to reflectance values, the backscattering coefficient is calculated during the radiometric calibration process. This coefficient is directly proportional to the reflectance. Thus, the histograms and raster files for this coefficient (Figs. 5 and 6) are similar to Figures 3 and 4. However, the backscattering coefficient is influenced by the incidence angle, as a result of Equation (3). For  $\lambda=532$  nm scan angle was degrees, for  $\lambda=1064$  nm: 60 degrees. For  $\lambda=1550$  nm the scan angle was restricted to 60 degrees.

$$\gamma = 4 \rho \cos\theta \quad (3)$$

where:  $\gamma$  is the backscattering coefficient,  
 $\rho$  is the reflectance,  
 $\theta$  is the incidence angle.

The histograms in Figure 5 therefore show a distribution similar to that in the reflectance histograms, but with values up to four times higher. The differences between the raster files for both factors are barely detectable; some influence of the incidence angle on backscattering coefficient can be seen only for the VUX data, in the south-east part of the study area.

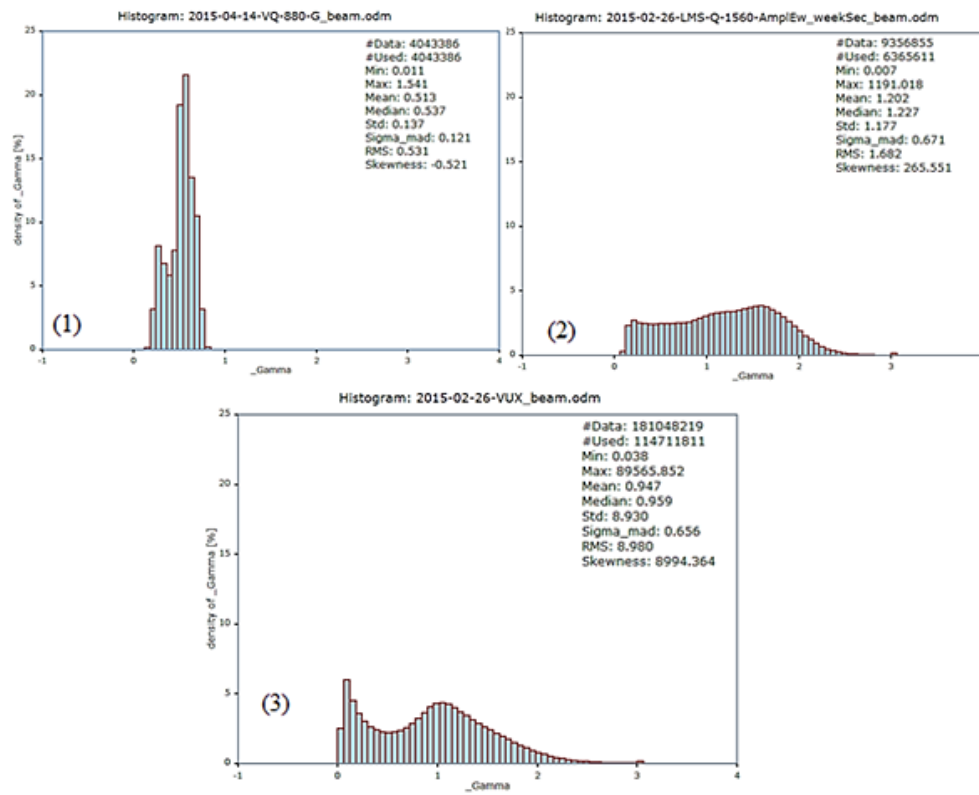


Fig. 5. Backscattering coefficient of each dataset: (1) bathymetric dataset; (2) infrared airborne dataset; (3) infrared UAV dataset

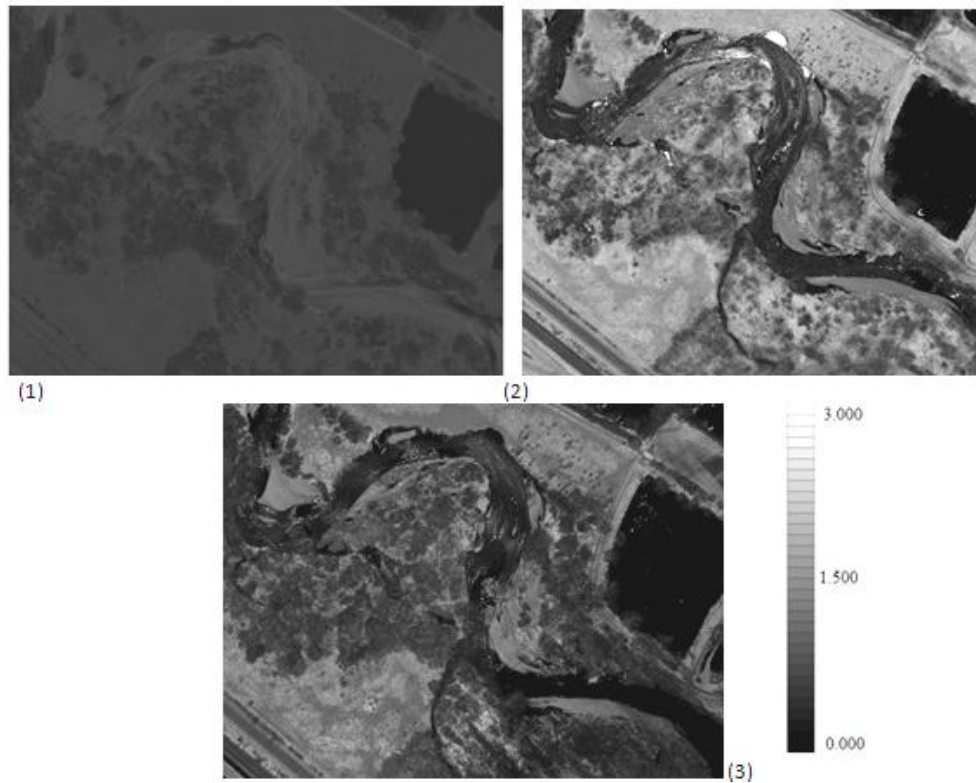


Fig. 6. Raster images presenting backscattering coefficient at each wavelength:  
(1)  $\lambda=532$  nm; (2)  $\lambda=1064$  nm (3)  $\lambda=1550$  nm

## 5. COMPARISON OF REFLECTANCE VALUES WITH SPECTRAL CHARACTERISTICS

The obtained reflectance values presented above provide information about the amount of reflected radiation. The radiometric properties of most objects have already been studied and presented as spectral characteristics (Fig. 7). In this section the calculated reflectance values are compared with spectral curves.

Several conclusions can be drawn from the reflectance values for each dataset. For instance, the reflectivity in the green spectrum is much lower for the dominant features of the study area (grassland, trees) than that in the infrared spectrum, and this is confirmed in Figure 7. For  $\lambda=532$  nm, the reflectance is much lower in comparison to the remaining part of the spectrum. For the bathymetric laser scanner, the median reflectance value is 0.16, thus tallying with the spectral characteristics. The reflectivity in the green spectrum is somewhat poorly diversified, and it is therefore difficult to consider the results separately for every object. For the infrared airborne scanning data, the calibrated intensity shows more variation. Vegetation reflects more radiation than other objects; according to the spectral curves, the reflectance can reach 55%–60%. From the histogram in Figure 3,

showing the results for  $\lambda=1064$  nm, it can be observed that there is a maximum in the distribution of values for reflectance at about 45%–50%, resulting from vegetation within the study area. However, the reflectance is somewhat lower than in the spectral characteristics, and this may have been caused by the season in which registration was carried out. The data were obtained at the end of February, when the trees were not in leaf, and thus the reflectance for vegetation is slightly lower than 60%. Nevertheless, the calibration results show that areas characterized by lower reflectance are clear. These are the ground areas near the river and, in the south-west part, the road and railway. According to Figure 7, these objects reflect less radiation in the infrared spectrum than vegetation. However, it is significant that soil reflectance increases with wavelength, as can also be seen from the raster images for the area near the river. The results show that in the third band ( $\lambda=1550$  nm), vegetation reflects less radiation than in the infrared airborne dataset and more than in the green spectrum, as confirmed by the spectral curves. Moreover, an analysis of both histograms and spectral characteristics shows that for UAV infrared data the reflectivity is higher than for the data captured with the bathymetric scanner, and the differences in object reflectance do not vary as much as for the airborne infrared data.

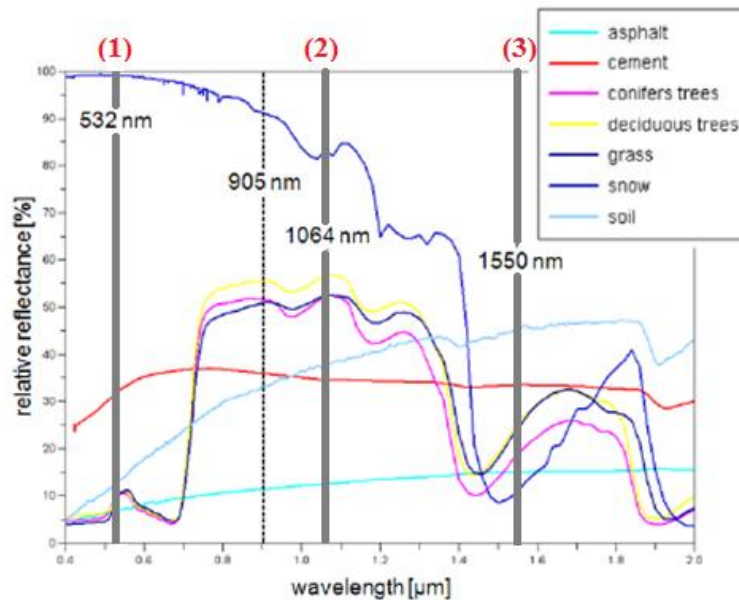


Fig. 7. Example of spectral characteristics representing reflectance values (based on Pfennigbauer and Ullrich, 2011)

To summarize, a comparison of calculated reflectance and spectral characteristics, used as reference information proved that radiometric calibration was conducted properly and multispectral laser scanning may be used as a source of both geometric and radiometric information. This data can be used to 3D classification and calculating vegetation indices which deliver information about vegetation condition. On Figure 8 a coloured composite of integrated point cloud is presented. The data were integrated so that each echo of one scan has the reflectance from the nearest echo of the second scan, stored as additional attribute.

According to Figure 8, such a composite shows the potential of the information which are delivered in high resolution multispectral laser data.

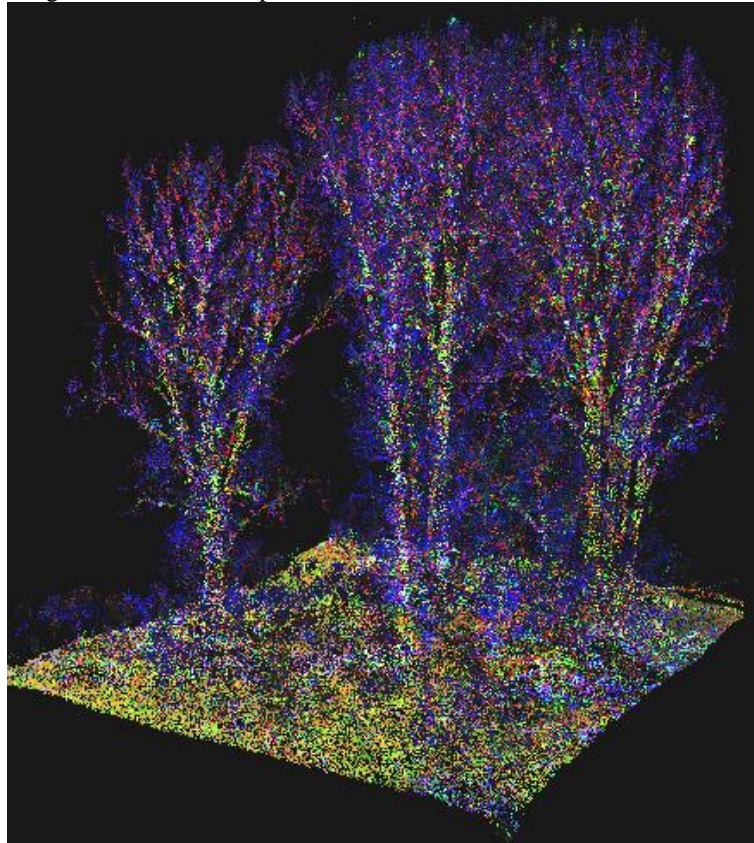


Fig. 8. Colour composite demonstrating the added value of the high resolution multispectral laser data

#### **ACKNOWLEDGENTS**

The author would like to thank RIEGL Laser Measurement Systems GmbH for providing the laser scanning data. This experiment was conducted with support from Dipl.-Ing. Dr. Techn. Gottfried Mandlbürger from the Vienna University of Technology.

#### **LITERATURE**

Baltsavias E.P., 1999. Airborne laser scanning: basic relations and formulas. *ISPRS Journal of Photogrammetry and Remote Sensing*, 54 (2/3), pp. 199–214.

Bakuła K., 2015. Multispectral airborne laser scanning – a new trend in the development of LiDAR technology. *Archiwum Fotogrametrii, Kartografii i Teledetekcji*, 27, pp. 25-44.

- Briese C., Pfennigbauer M., Lehner H., Ullrich A., Wagner W., Pfeifer N., 2012. Radiometric calibration of multi-wavelength airborne laser scanning data. *ISPRS Annals of the Photogrammetry, Remote Sensing and Spatial Information Sciences*, 1, 335-340
- Doneus M., Miholjek I., Mandlbürger G., Doneus N., Verhoeven G., Briese C., Presegbauer M., 2015. Airborne laser bathymetry for documentation of submerged archaeological sites in shallow water. *International Archives of the Photogrammetry, Remote Sensing and Spatial Information Science*, 40(5), pp. 99-107.
- Hemmler M., Weritz F., Schiemenz A., Grote A., Maierhofer, C., 2006. Multi-spectral data acquisition and processing techniques for damage detection on building surfaces. *International Archives of the Photogrammetry, Remote Sensing and Spatial Information Science*, 36, Part 5.
- Irish J. L., Lillycrop W. J., 1999. Scanning laser mapping of the coastal zone: the SHOALS system. *ISPRS Journal of Photogrammetry & Remote Sensing*, 54, pp. 123-129.
- Kaasalainen S., Hyyppä J., Litkey P., Hyyppä H., Ahokas E., Kukko A., Kaartinen H., 2007. Radiometric calibration of ALS intensity. *International Archives of the Photogrammetry, Remote Sensing*, 36, pp. 201-205.
- Lehner H., Briese C., 2010. Radiometric calibration of full-waveform airborne laser scanning data based on natural surfaces. *International Archives of Photogrammetry, Remote Sensing and Spatial Information Sciences*, 38 (Part 7B), pp. 360–365.
- Mandlbürger G., Pfennigbauer M., Riegl U., Haring A., Wieser M., Glira P., Winiwarter L., 2015a. Complementing airborne laser bathymetry with UAV-based lidar for capturing alluvial landscapes. *SPIE Remote Sensing*, pp. 96370A-96370A.
- Mandlbürger G., Glira P., Pfeifer N., 2015b. UAS-borne Lidar for Mapping Complex Terrain and Vegetation Structure. *GIM International*, 29(7), pp. 30-33.
- Mandlbürger G., Hauer C., Wieser M., Pfeifer N., 2015. Topo-bathymetric LiDAR for monitoring river morphodynamics and instream habitats—A case study at the Pielach River, *Remote Sensing*, 7(5), pp. 6160-6195.
- Pfennigbauer M., Ullrich A., 2011. Multi-Wavelength Airborne Laser Scanning. ILMF 2011, New Orleans.
- Pfeifer N., Mandlbürger G., Otepka J., Karel, W., 2014. OPALS—A framework for Airborne Laser Scanning data analysis. *Computers, Environment and Urban Systems*, 45, pp. 125-136.
- Wallace A., Nochol C., Woodhouse I., 2012. Recovery of forest canopy parameters by inversion of multispectral LiDAR data. *Remote Sensing*, 4(2), pp. 509-531.
- Wagner W., 2010. Radiometric calibration of small-footprint full-waveform airborne laser scanner measurements: Basic physical concepts. *ISPRS Journal of Photogrammetry and Remote Sensing*, 65(6), pp. 505-513.
- Wehr A., Lohr U., 1999. Airborne laser scanning – an introduction and overview. *ISPRS Journal of Photogrammetry & Remote Sensing*, 54, pp. 68-82.
- Wichmann V., Bremer M., Lindenberger J., Rutzinger M., Georges C., & Petrini-Monteferrri F., 2015. Evaluating the potential of multispectral airborne LiDAR for topographic mapping and land cover classification. *ISPRS Annals of the Photogrammetry, Remote Sensing and Spatial Information Sciences*, 1, pp. 113-119.

## KALIBRACJA RADIOMETRYCZNA DANYCH Z LOTNICZEGO SKANINGU LASEROWEGO

SŁOWA KLUCZOWE: lotniczy skaning laserowy, LiDAR, skaning multipiektralny, kalibracja radiometryczna, OPALS

### Streszczenie

Lotniczy skaning laserowy (ALS) jest szeroko wykorzystywaną technologią w pomiarach fotogrametrycznych. Na podstawie dyskretnej rejestracji punktów tworzone są m.in. numeryczne modele terenu (NMT), numeryczne modele pokrycia terenu (NMPT), modele 3D miast. Większość skanerów rejestrujących z pułapu lotniczego pozyskuje dane w zakresie bliskiej podczerwieni. Jednak od pewnego czasu można spotkać się z pojęciem skaningu multispektralnego, który polega na rejestracji danych w więcej niż jednym zakresie spektralnym. Oprócz zakresu podczerwonego ( $\lambda=1064$  nm), powszechne jest użycie skaningu batymetrycznego rejestrującego w zakresie zielonym oraz zakresie podczerwonym charakteryzującym się inną długością fali ( $\lambda=1500$  nm).

Aby móc korzystać z danych radiometrycznych, które dostarczane dzięki skaningowi multispektralnemu, niezbędne jest przeprowadzenie kalibracji radiometrycznej. Kalibracja radiometryczna jest kluczowym procesem przeprowadzanym podczas przetwarzania obrazów z pułapu satelitarnego w teledetekcji. Dzięki kalibracji niwelowany lub całkowicie wyeliminowany zostaje wpływ czynników zewnętrznych na otrzymane wartości radiometryczne. Mniej popularna, lecz również wskazana jest kalibracja radiometryczna w kontekście danych ze skaningu laserowego, kiedy to eliminowany zostaje wpływ m.in. zasięgu i kąta skanowania na rejestrowane wartości intensywności. Wynikiem kalibracji radiometrycznej są wartości współczynnika odbicia dla każdego echa, co wpływa na wzrost możliwości wykorzystania danych ze skaningu.

W powyższym artykule zaprezentowane zostały wyniki kalibracji radiometrycznej danych ze skaningu lotniczego. Analizowane dane pochodziły z trzech różnych sensorów, a każdy z nich charakteryzował się inną częstotliwością lasera: 532 nm (lotniczy skaner batymetryczny), 1064 nm (skaner lotniczy) oraz 1550 nm (skaner zamontowany na bezzałogowym statku powietrznym UAV). Wyniki kalibracji zaprezentowane zostały w postaci rastrów oraz histogramów, a następnie omówione zostały różnice między wartościami odbicia w poszczególnych zakresach. W ostatnim rozdziale przeprowadzone zostało porównanie otrzymanych wartości współczynnika odbicia z krzywymi spektralnymi dla wybranych obiektów.

Dane autorów / Authors details:

mgr inż. Magdalena Pilarska

e-mail: magdalena.pilarska@pw.edu.pl

Przesłano / Submitted 16.11.2016

Zaakceptowano / Accepted 21.12.2016